DOI: 10.22034/ijicmes.2025.228594

University of Hormozgan

International Journal of
Innovative Computational Methods
in Engineering Sciences
2025, * (*), **-**
journal homepage – cme.hormozgan.ac.ir

Scale-Dependent Buckling Analysis of Advanced Lightweight Nanocomposite Sandwich Beams Regarding Shear Deformation and Temperature Changes Effects

Ehsan Arshid [a,*]

[a] Faculty of Engineering, Mahallat Institute of Higher Education, Mahallat, Iran.

ARTICLE INFO

Keywords:
Buckling Analysis
Microbeams
Temperature Changes
Sandwich Structures
Graphene Nanoplatelets
Porous Materials

Received:
Revised:
Accepted:
Available online

ABSTRACT

In this study, the mechanical buckling of a Timoshenko sandwich microbeam is analysed, where the core is made of functionally graded porous materials, and the facesheets are composed of graphene platelets reinforced nanocomposites. The mechanical properties of the beam layers vary along the thickness direction based on defined functions, and the microstructure is subjected to thermal load. The governing equations are derived using the principle of virtual work and the variational method based on both first-order shear deformation and modified couple stress theories to capture the effect of shear deformation and scale. Navier's method is employed as an analytical solution for simply supported boundary conditions to obtain the critical buckling loads of the microbeam. The effects of various factors such as temperature changes, porosity coefficient, amount and dispersion type of reinforcing nanoparticles in the facesheets, elastic foundation parameters, and other important parameters are investigated and analysed. It is observed that increasing the porosity coefficient of the microbeam's core leads to a decrease in the critical buckling load. Moreover, based on the results, an increase in the mass fraction of reinforcing nanoparticles in the facesheets generally leads to an increase in the critical buckling load. The outcomes of this research can be used in the design of space and innovative structures.

1. Introduction

Beams are widely recognized as fundamental structural elements in engineering and have been extensively utilized in various scientific and industrial fields. In civil engineering, they are commonly incorporated into buildings, bridges, and frameworks where loads must be carried and transferred efficiently [1], [2], [3]. In mechanical engineering, their use is frequently observed in machine components, vehicle frames, and turbine blades, where strength, stiffness, and durability are required under dynamic and static loading conditions [4], [5], [6].

Different kinds of beams have been developed to address specific structural demands. For instance, simple beams are supported at their ends and are commonly subjected to bending under uniform or concentrated loads. Continuous beams span over two supports and have been adopted for enhanced structural efficiency and reduced deflections. Cantilever beams, fixed at one end and free at the other, are frequently employed in overhanging structures or components where unilateral support is necessary. Beams of varying cross-

* Corresponding author. Tel.: +98-864-853-2442; e-mail: e.arshid@mahallat.ac.ir; ehsanarshid@gmail.com

sections, such as I-beams or box beams, have been engineered to improve bending resistance while minimizing material usage.

Throughout engineering history, the behavior of beams under loads has been studied using different theories, including Euler–Bernoulli beam theory for slender beams and Timoshenko beam theory when shear deformation and rotary inertia cannot be neglected. In more advanced applications, such as aerospace structures or biomedical devices, functionally graded materials and composite beams have been introduced to optimize performance under complex loading and environmental conditions [7], [8], [9], [10].

Significant advantages have been associated with beam-type structures. They have been favored for their high load-bearing capacity relative to their weight and for their mechanical behavior's predictability, allowing for accurate modeling and design. Beams can also be fabricated from various materials, including metals, polymers, ceramics, and composite materials, allowing them to be tailored for specific mechanical, thermal, or environmental constraints.

Their applications have been extended beyond traditional construction and machinery. In robotics, beam-like elements have been integrated into lightweight structures that maintain flexibility and strength. In bioengineering, prosthetic limbs and implantable devices have been designed using beam principles to mimic the load-bearing function of bones. In the energy sector, beams have been incorporated into the structural framework of wind turbine blades and solar panel mounts to ensure stability and efficiency under variable conditions [11].

Beams have maintained their central role in engineering design across disciplines by being adaptable, structurally efficient, and easily analyzed using well-established mathematical models. Their continued development and refinement are driven by the demands of modern technologies and the availability of new materials.

Engineering has widely adopted sandwich structures due to their exceptional mechanical performance and lightweight characteristics. These structures consist of two strong and stiff face sheets bonded to a lightweight core, forming a configuration in which the face sheets primarily carry loads while the core provides separation and resists shear. In civil and mechanical engineering, sandwich beams have been increasingly utilized in structural components where high strength-to-weight ratios and enhanced bending stiffness are required [12], [13], [14]. Several types of sandwich beams have been developed based on core material and geometry. Cores from foam, honeycomb, corrugated, or lattice materials have been extensively employed. These cores are designed to be lightweight while maintaining stability under mechanical loads. Functionally graded and porous materials have also been introduced into the sandwich core design to improve thermal resistance, energy absorption, and vibration damping. In many cases, the face sheets are reinforced with composite materials or nanostructured additives to enhance strength and durability further [15], [16], [17].

In civil engineering, sandwich beams have been incorporated into bridge decks, floor systems, and façade elements, emphasizing structural performance and material efficiency. Their use in mechanical and aerospace engineering has been extended to aircraft wings, fuselage panels, and satellite structures, where weight reduction without compromising strength is essential. The automotive industry has also adopted sandwich structures in body panels and crash-absorbing zones, where impact resistance and energy absorption must be optimized.

The main advantages of sandwich beams are combining high stiffness, low weight, and excellent energy absorption capacity. Thermal insulation, acoustic damping, and resistance to fatigue and impact have been significantly improved in such structures. Furthermore, the ability to tailor material properties through layering and core selection has enabled sandwich beams to be adapted to a wide range of service conditions [18], [19], [20].

Analytical and numerical models have been developed to predict the behavior of sandwich beams under various loading and boundary conditions. Advanced theories, including higher-order shear deformation and nonlinear formulations, have been applied to accurately capture the influence of core compressibility, face wrinkling, and local buckling phenomena. Experimental validations have been conducted to confirm theoretical predictions and modern manufacturing techniques have allowed for their scalable production.

Advancements in material science and structural mechanics have driven the continued evolution of sandwich beam technology. Their multifunctionality, which includes structural support, energy management, and environmental adaptability, has ensured their relevance across diverse scientific and engineering disciplines.

Microstructures refer to miniature systems or components typically on the micrometer scale and often fabricated using microelectromechanical systems (MEMS) technology. These structures are commonly embedded within various devices and systems where extremely small sizes and high precision are required. Among the many types of microstructures, microbeams are widely recognized and have been extensively studied due to their versatile functionality and mechanical behavior.

Microbeams are slender structural elements whose dimensions are scaled down to the micrometer range. They are usually fabricated using photolithography, etching, and thin-film deposition techniques. Different materials, including silicon, polymers, and metals, are selected depending on the intended use. Once created, these beams are often integrated into larger systems where their mechanical properties, such as stiffness and vibrational characteristics, play a critical role [21], [22], [23].

Microbeam applications have been observed in a variety of fields. In sensors and actuators, microbeams have been utilized to detect physical quantities such as pressure, temperature, and acceleration. In optical systems, they have been employed to manipulate light paths by acting as tunable mirrors or diffraction elements. Within the biomedical sector, microbeams have been incorporated into devices for drug delivery, diagnostics, and tissue manipulation. Furthermore, their use has been extended to atomic force microscopy, where they function as cantilever arms capable of scanning surfaces at the nanoscale.

Several advantages have been associated with microbeams. Because of their small size, they have been found to require minimal power for actuation and to respond rapidly to external stimuli. Their fabrication in large numbers on a single substrate has enabled cost-effective mass production. Additionally, high sensitivity and reliability have been demonstrated in many applications, particularly in environments where compact and precise components are essential. Through the integration of microbeams, devices have been made more efficient, lightweight, and capable of performing tasks that would be challenging at larger scales.

Nanocomposite structures are materials composed of a matrix phase into which nanoscale reinforcements have been embedded. These reinforcements are typically dispersed within the base material to enhance its physical, mechanical, thermal, or electrical properties. Graphene nanoplatelets (GPLs) have been widely used among the various types of nanoscale fillers due to their remarkable intrinsic characteristics.

Significant improvements in mechanical strength, stiffness, and fracture resistance have been reported when nanocomposites are reinforced with graphene nanoplatelets. Owing to the two-dimensional structure of graphene and its high aspect ratio, load transfer between the matrix and the reinforcement is effectively facilitated. Moreover, excellent thermal and high electrical conductivity have been introduced into the host material by including GPLs. These enhancements have been observed even at relatively low filler contents, making GPLs especially attractive in weight-sensitive applications [24], [25], [26], [27].

Such nanocomposite structures have been applied across a broad range of industries. In the aerospace and automotive sectors, they have been employed to improve structural integrity while reducing overall weight.

Components have been fabricated in electronics using GPL-reinforced nanocomposites to achieve better thermal management and electromagnetic shielding. Biomedical devices and sensors have also been designed using these materials, where their biocompatibility and responsiveness have been favorably utilized. Their application has achieved enhanced barrier properties and durability in coatings and packaging.

The advantages provided by GPL reinforcements have been widely recognized. Enhanced material performance has been achieved without significantly altering processing methods, and compatibility with existing manufacturing technologies has been maintained. Furthermore, durability under mechanical loading, resistance to thermal degradation, and multifunctionality have all been improved, making these materials highly desirable for next-generation engineering systems.

Porous materials contain cavities filled with fluid, typically air or water. The solid part of these materials is known as the matrix or framework, which is usually a solid phase. Choosing a sandwich beam with a porous core can introduce novel and enhanced characteristics compared to previous studies [28], [29], [30]. Porosity is the most significant feature of porous materials, while other properties, such as permeability, tensile strength, and electrical conductivity, are related to the properties of the matrix and the fluid within the pores.

The concept of porous media is widely applicable across numerous scientific and engineering fields, such as filtration, soil mechanics, rock mechanics, petroleum engineering, tissue regeneration, construction engineering, geology, biology and biophysics, and materials engineering. For instance, porous materials can be utilized in land, rail, marine, and air transportation. They also find use in the biomedical industry, filters and separators, heat exchangers and coolers, and other crucial applications, emphasizing the importance of analyzing their properties.

Porous materials naturally occur in many substances, such as wood, cork, sponges, and bones. Beams, including turbine blades, are commonly used as key components in industrial parts. Various dynamic and static analyses can be conducted on such structures, including bending, buckling, free vibration, forced vibration, and wave propagation studies.

In 2016, Chen et al. [31] investigated the free and forced vibrations of functionally graded porous (FG) beams with symmetric and asymmetric porosity distributions, obtaining natural frequencies and transient dynamic deflections under different loading conditions. Magnucki and Stasiewicz [32] studied the elastic buckling of a porous beam with a rectangular cross-section made from isotropic porous material, whose properties varied across the thickness. Using a curved Timoshenko beam theory, Tseng et al. [33] employed a stiffness analysis method accounting for shear deformation and rotary inertia to determine the natural frequencies of multilayer curved beams. Although first-order shear deformation theories (FSDT) assume a constant shear deformation along the thickness, the accuracy of results is highly dependent on the selection of a shear correction factor. Furthermore, this theory suits thin and moderately thick beams but not thick ones. Matsunaga [34] showed that higher-order shear deformation theories provide more accurate predictions of natural frequencies for moderately thick laminated curved beams. Ahmed [35] evaluated the vibrational characteristics of sandwich beams using finite element analysis with three to five degrees of freedom per node, also assessing the effects of factors such as core-to-face density ratio, core stiffness, and core-to-face thickness ratio on the natural frequency. Using Green's functions, Sakiyama et al. [36] examined the free vibration of sandwich arches with elastic and viscoelastic cores under various boundary conditions. Rao et al. [37] proposed an analytical method based on a higher-order composite beam theory to evaluate the natural frequencies of composite and sandwich beams. Also, recently, other works on analyzing beams' mechanical performance with different material types have been published that can be seen in Refs. [22], [38], [39], [40].

Based on the literature review, it is evident that no prior research has been conducted on the mechanical buckling of porous sandwich microbeams with GPLs-reinforced coatings. Therefore, this study uses the Timoshenko beam model, the modified couple stress theory (MCST), and the principle of virtual work to derive the governing equations of a sandwich microbeam. Subsequently, the Navier method is employed to obtain an analytical solution for simply supported boundary conditions, and the influence of various parameters on the results is discussed and analyzed. The findings of this research can be applied to the design of space and smart structures.

2. Basic Relations

The beam under investigation is a three-layer microbeam. L denotes its length, the total thickness by h, and the origin of the coordinate system is considered at its bottom-left corner. The core of the beam is made of functionally graded porous material, while the facesheets are composed of GPLs-reinforced composite. The beam is also assumed to rest on an elastic foundation modeled using the Pasternak model. Furthermore, the properties of the three layers of the microbeam are considered to vary as a function of the beam's thickness.

To express the displacement components of the under-investigation beam, the Timoshenko beam theory is employed, in which the displacement components are described as follows [41]:

$$\begin{aligned} U(x,z) &= u(x) - z\frac{\partial w(x)}{\partial x} + \Phi(z)\varphi(x), \\ V(x,z) &= 0, \\ W(x,z) &= w(x) \end{aligned} \tag{1}$$

In this expression, U, V, and W represent the displacements of any point on the beam in the x-, y-, and z-directions, respectively, while u and w denote the displacements of the beam's mid-surface. Moreover, the function $\Psi(z)$ is defined based on the Timoshenko beam theory as follows:

$$\Phi(z) = z \tag{2}$$

The strain–displacement relations based on the linear terms of the von Kármán theory are expressed as follows:

$$\varepsilon_{xx} = \frac{\partial U(x,z)}{\partial x}, \qquad \varepsilon_{yy} = \frac{\partial V(x,z)}{\partial y},$$

$$\gamma_{xy} = \frac{\partial U(x,z)}{\partial y} + \frac{\partial V(x,z)}{\partial x}, \qquad \gamma_{xz} = \frac{\partial U(x,z)}{\partial z} + \frac{\partial W(x,z)}{\partial x}, \tag{3}$$

$$\gamma_{yz} = \frac{\partial V(x,z)}{\partial z} + \frac{\partial W(x,z)}{\partial y}$$

In classical continuum theory, the stress at any point depends on the strain at the same point and is independent of the strain at other points. The classical theory suits large dimensions, and theoretical analyses align with experimental results. However, in small dimensions such as micro or nano scales, research shows that the stress at any point is no longer dependent on the strain at that point alone. Instead, it is related to the strain across the entire body. This phenomenon is referred to as the size effect. In the coupled stress theory, there is only one non-classical coefficient, l_m, which has been used in other studies and utilized in this research. Based on the MCST, the strain energy of a material is expressed as follows [42]:

$$U_M = \frac{1}{2}\int_V (\sigma{:}\varepsilon + \mathrm{m}{:}\chi)\ \mathrm{dV} \tag{4}$$

In this relation, the subscript *M* refers to the MCST, and as previously mentioned, σ and ε are the stress and strain tensors, respectively. τ and κ represent the deviatoric part of the coupled stress tensor and the symmetric part of the curvature tensor, respectively, which are defined as follows [43]:

$$\mathrm{m} = 2l_m^2 \mu \chi, \tag{5}$$

$$\chi = \frac{1}{2}[\nabla\Theta + (\nabla\Theta)^T] \tag{6}$$

In the above relations, l_m is the small-scale parameter associated with the MCST, and μ is the Lame's parameter. Additionally, Θ is the rotation vector, for which the following holds:

$$\Theta = \frac{1}{2}\nabla \times \mathrm{u} \tag{7}$$

where u is the displacement vector.

The structural relations for each of the three layers of the microbeam are expressed as follows [44]:

$$\sigma_{ij} = Q_{ijkl}(\varepsilon_{kl} - \alpha \Delta T) \tag{8}$$

In this equation, ΔT and α are temperature changes and thermal expansion coefficient, respectively. Also, the components of the stiffness matrix are expressed in terms of the engineering properties for each layer.

To express the components of the stiffness matrix defined in Eq. (8), for the face sheets reinforced with graphene nanoparticles, we have:

$$Q_{11}^{t,b}(z) = \frac{[1 - \nu_{t,b}(z)]E_{t,b}(z)}{[1 + \nu_{t,b}(z)][1 - 2\nu_{t,b}(z)]}, \qquad Q_{55}^{t,b}(z) = \frac{E_{t,b}(z)}{2[1 + \nu_{t,b}(z)]} \tag{9}$$

To determine the effective elastic modulus in the nanocomposite facesheets, based on the Halpin-Tsai model, we have [45]:

$$E_{t,b}(z) = \frac{E_m}{8}[3\alpha_L + 5\alpha_W] \tag{10}$$

In this equation, E_m is the modulus of elasticity of the matrix, and also:

$$\alpha_L = \frac{1 + \zeta_L \eta_L V_{GPLs}}{1 - \eta_L V_{GPLs}}, \qquad \alpha_W = \frac{1 + \zeta_W \eta_W V_{GPLs}}{1 - \eta_W V_{GPLs}} \tag{11}$$

In the above relations, V_{GPLs} is the volume fraction of GPLs, and the other parameters are related to the geometry of the nanoparticles, which are expressed as follows:

$$\zeta_L = 2l_{GPLs}/h_{GPLs}, \qquad \zeta_W = 2\,w_{GPLs}/h_{GPLs}, \tag{12}$$

$$\eta_W = [(E_{GPLs}/E_m) - 1]/[(E_{GPLs}/E_m) + \zeta_W],$$
$$\eta_L = [(E_{GPLs}/E_m) - 1]/[(E_{GPLs}/E_m) + \zeta_L] \tag{13}$$

In the above relations, h, w, and l represent the thickness, width, and length of the GPLs, respectively. Additionally, the volume fraction of the GPLs can be determined using the following relation:

$$V_{GPLs} = \frac{g_{GPLs}(z)}{g_{GPLs}(z) + [\rho_{GPLs}/\rho_m][1 - g_{GPLs}(z)]} \tag{14}$$

In this relation, the density is denoted by ρ. Additionally, the mass fraction of the reinforcements is represented by g_{GPLs}, which is given by [46]:

$$g_{GPLs}(z)=\begin{cases}\left[4/h_f^2\right]\gamma_P W_{GPLs}\left(z\mp\left(h_c+h_f\right)/2\right)^2;\\ \left[0.5+\left(z\mp\left(h_c+h_f\right)/2\right)/h_f\right]\gamma_L W_{GPLs};\\ \gamma_U W_{GPLs};\end{cases} \tag{15}$$

These three models are the parabolic, linear, and uniform, respectively. Additionally, γ_P, γ_L, and γ_U are the variation indices corresponding to these three GPLs distribution models, which are presented in Table 1 for different values of GPLs.

Table 1. GPLs' gradient index based on their values for different dispersion patterns [46].

GPLs' Percentage	γ_U	γ_L	γ_P
0	0	0	0
1/3	1/3	2/3	1
1	1	2	3

Additionally, other properties of the facesheets, such as the coefficient of thermal expansion and Poisson's ratio, are determined using the rule of mixture based on the following relations:

$$\nu_{t,b}(z)=\nu_{GPLs}V_{GPLs}+\nu_m V_m, \tag{16}$$

$$\alpha_{t,b}(z)=\left[V_{GPLs}E_{GPLs}\alpha_{GPLs}+V_m E_m\alpha_m\right]/\left[V_{GPLs}E_{GPLs}+V_m E_m\right] \tag{17}$$

In order to obtain the components of the stiffness matrix introduced in Eq. (8) for the porous core, we have:

$$Q_{11}^c(z)=\frac{E(z)}{1-\nu^2}, \qquad Q_{55}^c(z)=\frac{E(z)}{2(1+\nu)} \tag{18}$$

In this study, three types of porosity distribution are considered. Thus, the mechanical properties of the porous material can vary based on the following three functions [47]:

a) *Nonlinear symmetric porosity distribution*:

$$E_c(z)=E_1\left(1-e_0\cos\left(\frac{\pi z}{h_c}\right)\right), \tag{19}$$

b) *Nonlinear asymmetric porosity distribution*:

$$E_c(z)=E_1\left(1-e_0\cos\left(\frac{\pi z}{h_c}+\frac{\pi}{4}\right)\right), \tag{20}$$

In this relation, E_1 and E_0 represent Young's modulus's maximum and minimum values, respectively.

c) Uniform porosity distribution:

$$E_c=E_0(1-e_0\chi), \tag{21}$$

In which:

$$\chi=\frac{1}{e_0}-\frac{1}{e_0}\left(\frac{2}{\pi}\sqrt{1-e_0}-\frac{2}{\pi}+1\right)^2 \tag{22}$$

Also, Fig. 1 shows three distinct void distribution patterns [47].

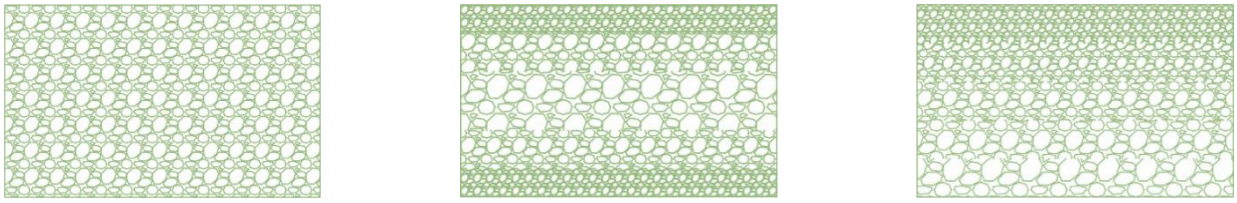

Uniform **Symmetric** **Asymmetric**

Fig. 1. Distribution patterns of pores.

Eq. (23) also expresses the relationship between Young's and shear modulus.

$$G_c(z) = E_c(z)/2(1+\nu_c), \tag{23}$$

$$e_0 = 1 - E_2/E_1 \tag{24}$$

e_0 and e_m are the porosity coefficients and mass densities, respectively. Using the above relations, it can be concluded that:

$$e_m = 1 - \sqrt{1 - e_0} \tag{25}$$

3. Derivation Procedure of the Governing Equilibrium Equations

In order to obtain the governing equations for the microbeam under analysis, the principle of virtual work is used [48]:

$$\delta[W - U] = 0 \tag{26}$$

Based on this principle, the difference between the changes in strain energy and external work is always equal to zero. Therefore, the strain energy must first be calculated to apply this principle. To obtain the strain energy of the microbeam, the following relation is used:

$$U = \frac{1}{2}\iiint \{\sigma_{xx}\varepsilon_{xx} + \sigma_{xz}\gamma_{xz} + 2m_{xy}\chi_{xy} + 2m_{yz}\chi_{yz}\}\,\mathrm{d}V \tag{27}$$

The work done by external forces in this study includes the work due to thermal load, in-plane buckling load, and the work done by the Pasternak foundation. To calculate the work done by the Pasternak elastic foundation, we have [49]:

$$W_{found.} = \frac{1}{2}\int \left[-\left(K_W w(x) - K_G \nabla^2 w(x)\right) w(x)\right] \mathrm{dx} \tag{28}$$

In the above relation, K_W is the Winkler foundation stiffness coefficient, and K_G is the shear layer stiffness coefficient.

The external work due to thermal load can be written as follows [50]:

$$W_{Thermal\ load} = \frac{1}{2}\int_x \left[N_T \left(\frac{\partial w(x)}{\partial x}\right)^2\right] \mathrm{dx} \tag{29}$$

In this relation, N_T is the thermal force applied in the x-direction, which is given by:

$$N_T = \int_z Q_{11}\alpha\Delta T\,\mathrm{d}z \tag{30}$$

And for the work done by the in-plane buckling load, we also have:

$$W_{in-plane} = \frac{1}{2}\int_x \left[N_x \left(\frac{\partial w(x)}{\partial x} \right)^2 \right] \mathrm{dx} \tag{31}$$

Finally, by substituting Eqs. (27)-(31) into Eq. (26), the governing equilibrium equations for the sandwich microbeam under investigation are obtained as follows:

$$\delta u:$$
$$-\frac{\partial}{\partial x} N_{xx} = 0, \tag{32}$$

$$\delta w:$$
$$-\frac{\partial^2}{\partial x^2} M_{xx} - \frac{\partial^2}{\partial x^2} R_1 - K_W w + K_G \frac{\partial^2}{\partial x^2} w + N_T \frac{\partial^2}{\partial x^2} w + N_x \frac{\partial^2}{\partial x^2} w = 0, \tag{33}$$

$$\delta \varphi:$$
$$-\frac{\partial}{\partial x} H_{xx} + P_x - \frac{1}{2}\frac{\partial}{\partial x} R_2 + \frac{1}{2} R_3 = 0 \tag{34}$$

The quantities used in the above equations are described as follows:

$$\begin{aligned} \{N_{xx} \quad M_{xx} \quad H_{xx}\} &= \int_z \sigma_{xx} \{1 \quad z \quad \Phi(z)\} \, \mathrm{dz}, \\ P_x &= \int_z \sigma_{xz} \frac{d}{dz} \Phi(z) \, \mathrm{dz}, \\ \{R_1 \quad R_2\} &= \int_z m_{xy} \left\{ 1 \quad \frac{d}{dz} \Phi(z) \right\} \mathrm{dz}, \\ R_3 &= \int_z m_{yz} \frac{d^2}{dz^2} \Phi(z) \, \mathrm{dz} \end{aligned} \tag{35}$$

In order to obtain the critical buckling loads, the Navier method is used as an analytical approach to solve the differential equations for the boundary conditions of a simply supported beam at both ends. To this end, the displacement components are assumed as follows [51]:

$$\begin{Bmatrix} u \\ w \\ \varphi \end{Bmatrix} = \sum_{m=1}^{\infty} \begin{Bmatrix} U_m \cos(\beta x) \\ W_m \sin(\beta x) \\ \Phi_m \cos(\beta x) \end{Bmatrix} \tag{36}$$

By rewriting Eqs. of motion (32)-(34) in terms of displacement components and substituting Eq. (36) into them, these relations can finally be expressed in the following matrix form:

$$\left([A] - N_{cr} [K_g] \right) \{d\} = 0 \tag{37}$$

By solving the above eigenvalue problem, the critical buckling loads will be obtained.

4. Results and Discussion

The results and the effect of various factors on the critical buckling load of the structure under investigation are presented. For this purpose, the porous core is made of SUS304, and the facesheets are made of Epoxy reinforced with GPLs. The mechanical and thermal properties of these materials are available in Refs. [45], [52].

It is worth noting that the porosity distribution is considered symmetric, and the distribution of GPLs is linear unless explicitly stated otherwise. Fig. 2 examines the effect of changes in the porosity coefficient and the length scale parameter on the critical buckling load. This figure shows that an increase in the length scale parameter leads to increased critical buckling load due to increased structural stiffness. The enhancement of the results with an increase in the dimensionless material length-scale parameter within the framework of the MCST can be attributed to the incorporation of size-dependent effects that are not captured by classical continuum theories. As the length-scale parameter increases, the material's resistance to deformation at smaller scales is strengthened due to the influence of the additional material length characteristic, which accounts for the internal material microstructure. This increased resistance effectively stiffens the microbeam, particularly in bending and shear, thereby raising its overall stability under compressive loads. Consequently, higher critical buckling loads are predicted when the length-scale parameter is enlarged. Additionally, it is observed that as the porosity coefficient increases, the critical buckling load decreases. The observed reduction in critical buckling loads with an increase in the porosity coefficient of the core from 0 to 0.8 can be physically justified by the degradation of the core's mechanical properties due to the increased presence of voids. As the porosity level rises, a larger fraction of the core volume is occupied by pores rather than solid material, decreasing the effective stiffness and load-bearing capacity of the core layer. Consequently, the overall structural rigidity of the sandwich microbeam is diminished. Since the core plays a significant role in resisting transverse shear and stabilizing the beam against buckling, a weakened core contributes less effectively to maintaining structural stability under compressive loads. As a result, lower critical buckling loads are predicted.

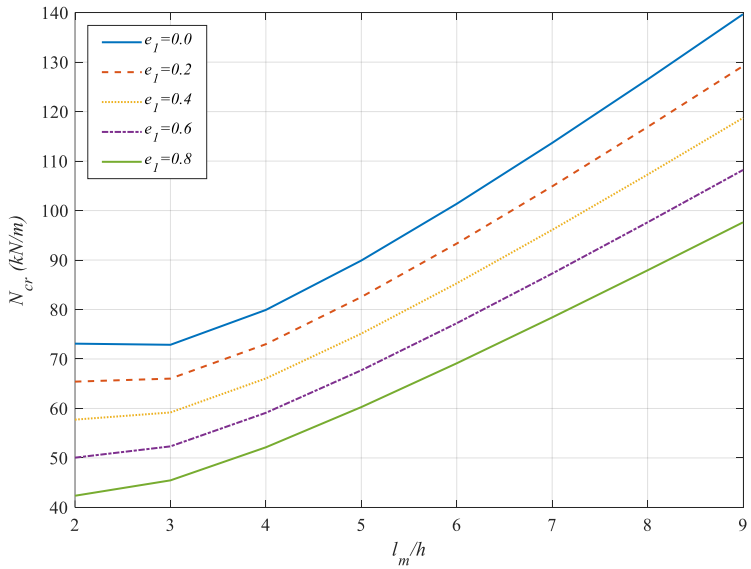

Fig. 2. Effect of the material length-scale parameter and porosity coefficient on the critical buckling loads.

Fig. 3 also examines the effect of increasing the porosity coefficient for the three types of porosity distributions studied. It can be observed that an increase in the porosity coefficient has a significant effect on reducing the critical buckling load for the two types of asymmetric and uniform porosity distributions, whereas it has a much smaller effect on the critical buckling load in the symmetric case. The variation in critical buckling load values among different porosity distribution patterns can be explained by how material stiffness is distributed through the core's thickness. When a symmetric porosity distribution is employed, the material is arranged to concentrate higher stiffness regions near the facesheets, where bending stresses are

most significant. This configuration allows the core to resist deformation more effectively and contributes to an overall increase in structural rigidity, resulting in higher critical buckling loads. In contrast, a uniform porosity distribution leads to an even reduction in stiffness throughout the core, including regions where mechanical resistance is most needed. As a result, the structure becomes less capable of withstanding compressive forces, and lower critical buckling loads are obtained.

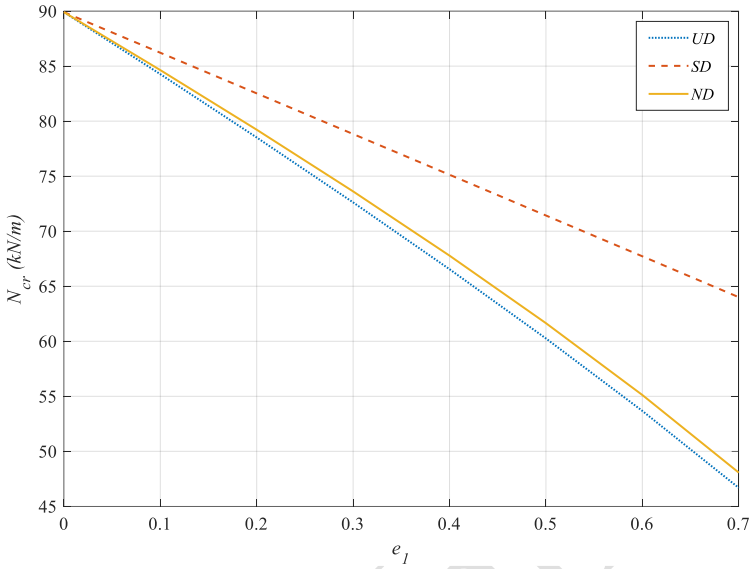

Fig. 3. Effect of the porosity coefficient and distribution patterns on the critical buckling loads.

In Fig. 4, the effect of the presence or absence and the distribution of GPLs along the thickness of the facesheets is examined. It is observed that if the presence of reinforcing nanoparticles is neglected, the critical buckling load is at its lowest value. However, adding GPLs reinforcements strengthens the structure, and the critical buckling load increases. It is also observed that the effect of adding GPLs is much more significant when they are distributed in a parabolic manner compared to the other two distributions. The enhancement of the results with an increase in the mass fraction of GPLs can be attributed to the superior mechanical properties of the reinforcing nanoparticles. As the GPL content is increased within the facesheets, the effective stiffness and strength of the nanocomposite layers are improved due to the high aspect ratio and exceptional elastic modulus of the graphene platelets. This enhancement allows the facesheets to resist higher compressive stress and deformation levels, leading to a more stable structural response. Consequently, higher critical buckling loads are predicted when the mass fraction of GPLs is increased.

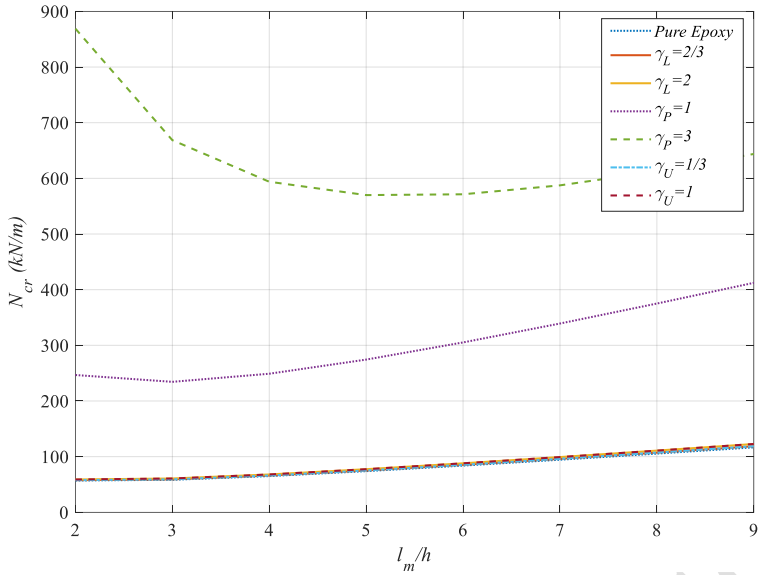

Fig. 4. Effect of adding GPLs to the facesheets and also, their dispersion patterns on the critical buckling loads.

In Fig. 5, two geometric characteristics of the GPLs are discussed. First is the length-to-width ratio, where it is observed that the critical buckling load decreases as this ratio increases. The reduction in the result with an increase in the length-to-width ratio of the GPLs can be explained by the change in the reinforcement distribution within the facesheets. As the length-to-width ratio increases, the GPLs tend to align more in a direction that reduces their effectiveness in resisting buckling. The elongated shape of the platelets may lead to a more pronounced alignment in the material, which can reduce the uniformity of the reinforcement and lead to less effective load transfer across the structure. This misalignment can lower the overall stiffness of the facesheets, thereby reducing the critical buckling load. Then, the thickness-to-length ratio is also observed and as this ratio increases, the critical buckling load decreases. The reduction in the results with an increase in the thickness-to-length ratio of the GPLs can be attributed to the increased resistance to deformation in the direction of the platelets' thickness. As the thickness of the GPLs increases relative to their length, the contribution of the platelets to the reinforcement becomes less effective in enhancing the overall stiffness of the facesheets. This is because thicker platelets may exhibit lower flexibility and bonding efficiency within the matrix material, reducing the ability to distribute stresses effectively across the structure. Consequently, the structural resistance to buckling is diminished, leading to lower critical buckling loads.

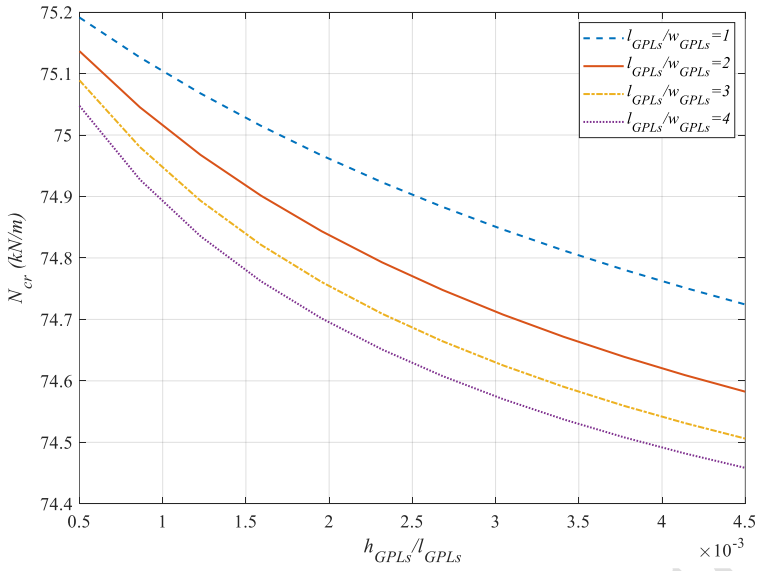

Fig. 5. Effect of the GPLs' geometrical parameters on the critical buckling loads.

The effect of environmental temperature changes is examined in Fig. 6. As observed, as the temperature increases, the structure's stiffness decreases, and consequently, the critical buckling load decreases. The temperature-dependent softening of the material properties can explain the reduction in the results with an increase in temperature changes. As the temperature rises, the material's stiffness generally decreases due to the increased atomic vibrations, which weaken the interatomic bonds. This reduction in stiffness leads to a decrease in the structural resistance to deformation under compressive loads. As a result, the microbeam becomes more susceptible to buckling, and the critical buckling loads are reduced when temperature changes are introduced. This behavior is valid for all the porosity coefficients studied.

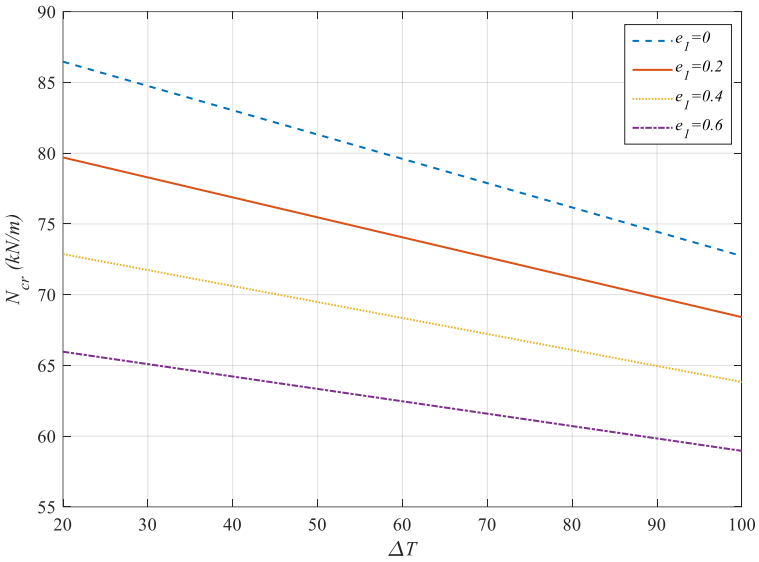

Fig. 6. Effect of temperature variations on the critical buckling loads.

As mentioned, the structure under investigation is placed on an elastic foundation of the Pasternak type, which includes springs and shear layers. Figs. 7 and 8 examine the effect of the Winkler spring coefficient

and the shear layer coefficient. It is observed that as both of these parameters increase, the critical buckling load increases. The enhancement in the results with an increase in both the springs and shear layer parameters of the Pasternak elastic foundation can be attributed to the increased support provided by the foundation. As the stiffness of both the spring and shear layers increases, the foundation becomes more effective in resisting vertical displacements and distributing the applied loads more uniformly across the microbeam. This enhanced foundation stiffness provides greater structural stability, reducing the likelihood of buckling under compressive forces. Consequently, the microbeam's overall resistance to deformation improves, leading to higher critical buckling loads. It can be concluded that adding the Pasternak foundation to the structure enhances its stiffness and increases its critical buckling load.

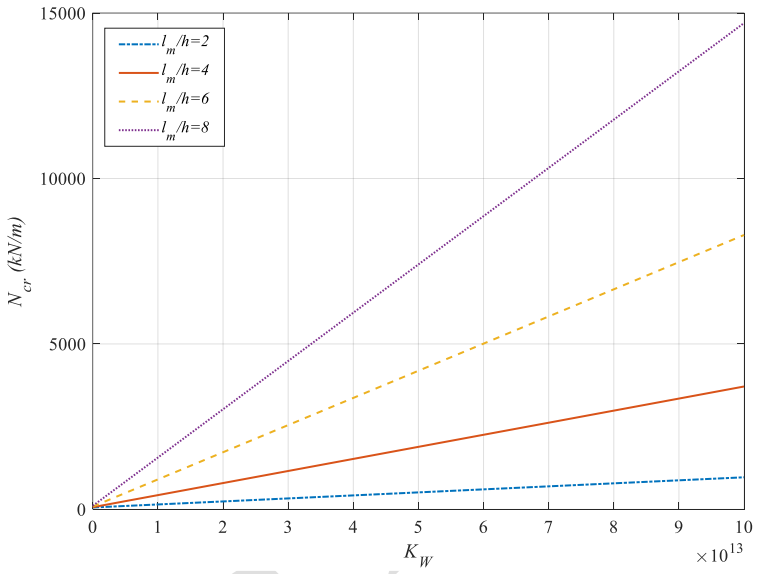

Fig. 7. Effect of the springs' parameter of the elastic foundation on the critical buckling loads.

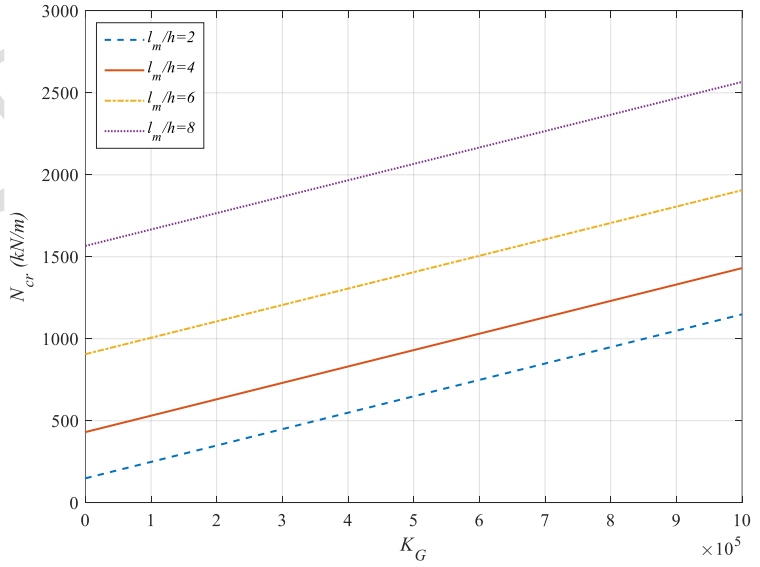

Fig. 8. Effect of the shear layer parameter of the elastic foundation on the critical buckling loads.

5. Conclusions

This study analyzes the mechanical buckling of a sandwich microbeam made of a functionally graded porous core, and GPLs-reinforced composite faces under the thermal loading and boundary condition of simply supported beam on both ends, based on the Timoshenko beam theory and MCST. First, the governing equations of the beam were derived using the virtual work principle. Then, these equations were solved analytically using the Navier method. Finally, the critical buckling load of the beam was obtained, and the effects of various factors were examined. The results are summarized as follows:

- The addition of reinforcing GPLs to the faces increases the critical buckling load.
- The critical buckling load generally decreases with an increase in the porosity coefficient.
- Among different considered patterns of porosity distribution, the symmetric pattern leads to the maximum, and the uniform pattern leads to the minimum values of critical buckling loads.
- The trend of the effect of the shear layer coefficient and Winkler coefficient on the critical buckling load shows that with the increase in these coefficients, the critical buckling load also increases, with a more significant increase observed for the shear layer coefficient.
- Increasing the material length-scale parameter of MCST leads to enhanced results.
- Also, increasing the length-to-width and thickness-to-length ratios of the GPLs reduces the critical buckling loads.
- An increase in temperature leads to a decrease in the critical buckling load.

References

[1] M. Sitar, F. Kosel, and M. Brojan, “Large deflections of nonlinearly elastic functionally graded composite beams,” *Arch. Civ. Mech. Eng.*, vol. 14, no. 4, pp. 700–709, Aug. 2014, doi: 10.1016/j.acme.2013.11.007.

[2] A. Mesbah, Z. Belabed, K. Amara, A. Tounsi, A. A. Bousahla, and F. Bourada, “Formulation and evaluation a finite element model for free vibration and buckling behaviours of functionally graded porous (FGP) beams ,” *Struct. Eng. Mech.*, vol. 86, no. 3, p. 309, May 2023, doi: 10.12989/SEM.2023.86.3.291.

[3] T. Q. Hung, D. M. Duc, T. M. Tu, L. X. Dung, and C. N. Bao, “Static and dynamic behaviour of sandwich beams with porous core: Experiment and moving least squares mesh-free analysis,” *J. Sci. Technol. Civ. Eng. - HUCE*, vol. 18, no. 1, pp. 39–54, Mar. 2024, doi: 10.31814/stce.huce2024-18(1)-04.

[4] M. Sobhy and A. M. Zenkour, “The modified couple stress model for bending of normal deformable viscoelastic nanobeams resting on visco-Pasternak foundations,” *Mech. Adv. Mater. Struct.*, vol. 27, no. 7, pp. 525–538, Apr. 2020, doi: 10.1080/15376494.2018.1482579.

[5] H. Bi, B. Wang, Z. Deng, and S. Wang, “Effects of thermo-magneto-electro nonlinearity characteristics on the stability of functionally graded piezoelectric beam,” *Appl. Math. Mech.*, vol. 41, no. 2, pp. 313–326, Jan. 2020, doi: 10.1007/s10483-020-2570-9.

[6] M. M. Kheirikhah, M. Ghiasvand, S. Gohery, and C. Burvill, “Free Vibration Analysis of Composite Sandwich Beams Reinforced by Functionally Graded Graphene Nanoplatelets,” *Mech. Compos. Mater.*, vol. 59, no. 5, pp. 959–976, Nov. 2023, doi: 10.1007/s11029-023-10145-3.

[7] F. Ebrahimi and M. Mokhtari, “Transverse vibration analysis of rotating porous beam with functionally graded microstructure using the differential transform method,” *J. Brazilian Soc. Mech. Sci. Eng.*, vol. 37, no. 4, pp. 1435–1444, Jul. 2015, doi: 10.1007/s40430-014-0255-7.

[8] D. Chen, S. Kitipornchai, and J. Yang, “Nonlinear free vibration of shear deformable sandwich beam with a functionally graded porous core,” *Thin-Walled Struct.*, vol. 107, pp. 39–48, Oct. 2016, doi: 10.1016/j.tws.2016.05.025.

[9] A. Omidi Soroor, M. Asgari, and H. Haddadpour, “Effect of axially graded constraining layer on the free vibration properties of three layered sandwich beams with magnetorheological fluid core,” *Compos. Struct.*, vol. 255, no. August 2020, p. 112899, 2021, doi: 10.1016/j.compstruct.2020.112899.

[10] Z. Q. Lu, F. Y. Zhang, H. L. Fu, H. Ding, and L. Q. Chen, “Rotational nonlinear double-beam energy harvesting,” *Smart Mater. Struct.*, vol. 31, no. 2, p. 025020, Dec. 2021, doi: 10.1088/1361-665X/AC4579.

[11] S. Amir, Z. Soleimani-Javid, and E. Arshid, “Size-dependent free vibration of sandwich micro beam with porous core

subjected to thermal load based on SSDBT," *ZAMM Zeitschrift fur Angew. Math. und Mech.*, vol. 99, no. 9, p. e201800334, Sep. 2019, doi: 10.1002/zamm.201800334.

[12] E. Arshid and S. Amir, "Size-dependent vibration analysis of fluid-infiltrated porous curved microbeams integrated with reinforced functionally graded graphene platelets face sheets considering thickness stretching effect," *Proc. Inst. Mech. Eng. Part L J. Mater. Des. Appl.*, vol. 235, no. 5, pp. 1077–1099, Jan. 2021, doi: 10.1177/1464420720985556.

[13] Y. Liu, S. Su, H. Huang, and Y. Liang, "Thermal-mechanical coupling buckling analysis of porous functionally graded sandwich beams based on physical neutral plane," *Compos. Part B Eng.*, vol. 168, pp. 236–242, Jul. 2019, doi: 10.1016/j.compositesb.2018.12.063.

[14] R. Patil, S. Joladarashi, and R. Kadoli, "Effect of porosity and viscoelastic boundary conditions on FG sandwich beams in thermal environment: Buckling and vibration studies," *Structures*, vol. 56, p. 105001, Oct. 2023, doi: 10.1016/j.istruc.2023.105001.

[15] F. Allahkarami and M. Nikkhah-Bahrami, "The effects of agglomerated CNTs as reinforcement on the size-dependent vibration of embedded curved microbeams based on modified couple stress theory," *Mech. Adv. Mater. Struct.*, vol. 25, no. 12, pp. 995–1008, Sep. 2018, doi: 10.1080/15376494.2017.1323144.

[16] Z. Khoddami Maraghi and E. Arshid, "On the vibrational behavior of variable thickness FG porous beams with graphene-reinforced nanocomposite facesheets," *Acta Mech.*, Jun. 2024, doi: 10.1007/s00707-024-03987-y.

[17] O. Polit, C. Anant, B. Anirudh, and M. Ganapathi, "Functionally graded graphene reinforced porous nanocomposite curved beams: Bending and elastic stability using a higher-order model with thickness stretch effect," *Compos. Part B Eng.*, vol. 166, pp. 310–327, Jun. 2019, doi: 10.1016/j.compositesb.2018.11.074.

[18] R. Moradi-Dastjerdi, K. Behdinan, B. Safaei, and Z. Qin, "Buckling behavior of porous CNT-reinforced plates integrated between active piezoelectric layers," *Eng. Struct.*, vol. 222, 2020, doi: 10.1016/j.engstruct.2020.111141.

[19] M. Khorasani, Z. Soleimani-Javid, E. Arshid, L. Lampani, and Ö. Civalek, "Thermo-elastic buckling of honeycomb micro plates integrated with FG-GNPs reinforced Epoxy skins with stretching effect," *Compos. Struct.*, vol. 258, pp. 1–28, 2021, doi: 10.1016/j.compstruct.2020.113430.

[20] E. Arshid, H. Arshid, S. Amir, and S. B. Mousavi, "Free vibration and buckling analyses of FG porous sandwich curved microbeams in thermal environment under magnetic field based on modified couple stress theory," *Arch. Civ. Mech. Eng.*, vol. 21, no. 1, p. 6, Mar. 2021, doi: 10.1007/s43452-020-00150-x.

[21] S. S. Mirjavadi, B. Mohasel Afshari, N. Shafiei, S. Rabby, and M. Kazemi, "Effect of temperature and porosity on the vibration behavior of two-dimensional functionally graded micro-scale Timoshenko beam," *J. Vib. Control*, vol. 24, no. 18, pp. 4211–4225, Sep. 2018, doi: 10.1177/1077546317721871.

[22] B. Akgöz and Ö. Civalek, "Bending analysis of embedded carbon nanotubes resting on an elastic foundation using strain gradient theory," *Acta Astronaut.*, vol. 119, pp. 1–12, 2016, doi: https://doi.org/10.1016/j.actaastro.2015.10.021.

[23] W. Zhang, H. Ma, and Y. Wang, "Stability and vibration of nanocomposite microbeams reinforced by graphene oxides using an MCST-based improved shear deformable computational framework," *Acta Mech.*, Dec. 2022, doi: 10.1007/s00707-022-03467-1.

[24] E. Arshid, S. Amir, and A. Loghman, "Thermal buckling analysis of FG graphene nanoplatelets reinforced porous nanocomposite MCST-based annular/circular microplates," *Aerosp. Sci. Technol.*, vol. 111, p. 106561, Apr. 2021, doi: 10.1016/j.ast.2021.106561.

[25] E. Arshid, M. A. Ghorbani, M. J. Momeni Nia, Ö. Civalek, and A. Kumar, "Thermo-elastic buckling behaviors of advanced fluid-infiltrated porous shells integrated with GPLs-reinforced nanocomposite patches," *Mech. Adv. Mater. Struct.*, pp. 1–17, Aug. 2023, doi: 10.1080/15376494.2023.2251015.

[26] C. Tao and T. Dai, "Isogeometric analysis for postbuckling of sandwich cylindrical shell panels with graphene platelet reinforced functionally graded porous core," *Compos. Struct.*, vol. 260, p. 113258, Mar. 2021, doi: 10.1016/j.compstruct.2020.113258.

[27] S. Yaqoob, Z. Ali, A. D'Amore, A. Lo Schiavo, A. Petraglia, and M. Rubino, "Enhanced Mechanical and Electrical Performance of Epoxy Nanocomposites Through Hybrid Reinforcement of Carbon Nanotubes and Graphene Nanoplatelets: A Synergistic Route to Balanced Strength, Stiffness, and Dispersion," *J. Compos. Sci.*, vol. 9, no. 7, p. 374, Jul. 2025, doi: 10.3390/jcs9070374.

[28] F. Rasooli Jazi, S. Amir, and E. Arshid, "Vibration analysis of asymmetric sandwich rotating FG porous discs coated with agglomerated nanocomposite facesheets," *Arch. Civ. Mech. Eng.*, vol. 24, no. 4, p. 201, Jul. 2024, doi: 10.1007/s43452-

024-01009-1.

[29] V. Kumar, S. J. Singh, V. H. Saran, and S. P. Harsha, "Vibration characteristics of porous FGM plate with variable thickness resting on Pasternak's foundation," *Eur. J. Mech. A/Solids*, vol. 85, p. 104124, Jan. 2021, doi: 10.1016/j.euromechsol.2020.104124.

[30] S. J. Singh and S. P. Harsha, "Thermo-mechanical analysis of porous sandwich S-FGM plate for different boundary conditions using Galerkin Vlasov's method: A semi-analytical approach," *Thin-Walled Struct.*, vol. 150, p. 106668, 2020, doi: https://doi.org/10.1016/j.tws.2020.106668.

[31] D. Chen, J. Yang, and S. Kitipornchai, "Free and forced vibrations of shear deformable functionally graded porous beams," *Int. J. Mech. Sci.*, vol. 108–109, pp. 14–22, Apr. 2016, doi: 10.1016/j.ijmecsci.2016.01.025.

[32] K. Magnucki and P. Stasiewicz, "Elastic buckling of a porous beam," *J. Theor. Appl. Mech.*, vol. 42, no. 4, pp. 859–868, 2004, Accessed: Jan. 08, 2021. [Online]. Available: http://www.ptmts.org.pl/jtam/index.php/jtam/article/view/v42n4p859

[33] Y. P. Tseng, C. S. Huang, and M. S. Kao, "In-plane vibration of laminated curved beams with variable curvature by dynamic stiffness analysis," *Compos. Struct.*, vol. 50, no. 2, pp. 103–114, Oct. 2000, doi: 10.1016/S0263-8223(00)00003-9.

[34] H. Matsunaga, "Free vibration and stability of laminated composite circular arches subjected to initial axial stress," *J. Sound Vib.*, vol. 271, no. 3–5, pp. 651–670, Apr. 2004, doi: 10.1016/S0022-460X(03)00298-0.

[35] K. M. Ahmed, "Free vibration of curved sandwich beams by the method of finite elements," *J. Sound Vib.*, vol. 18, no. 1, pp. 61–74, Sep. 1971, doi: 10.1016/0022-460X(71)90631-6.

[36] T. Sakiyama, H. Matsuda, and C. Morita, "Free vibration analysis of sandwich arches with elastic or viscoelastic core and various kinds of axis-shape and boundary conditions," *J. Sound Vib.*, vol. 203, no. 3, pp. 505–522, Jun. 1997, doi: 10.1006/jsvi.1996.0900.

[37] M. Kameswara Rao, Y. M. Desai, and M. R. Chitnis, "Free vibrations of laminated beams using mixed theory," *Compos. Struct.*, vol. 52, no. 2, pp. 149–160, May 2001, doi: 10.1016/S0263-8223(00)00162-8.

[38] S. Amir, Z. Soleimani-Javid, and E. Arshid, "Size-dependent free vibration of sandwich micro beam with porous core subjected to thermal load based on SSDBT," *ZAMM Zeitschrift fur Angew. Math. und Mech.*, vol. 99, no. 9, pp. 1–21, 2019, doi: 10.1002/zamm.201800334.

[39] F. Hou, S. Wu, Z. Moradi, and N. Shafiei, "The computational modeling for the static analysis of axially functionally graded micro-cylindrical imperfect beam applying the computer simulation," *Eng. Comput.*, vol. 38, no. 4, pp. 3217–3235, Oct. 2021, doi: 10.1007/S00366-021-01456-X/METRICS.

[40] H. Hu, T. Yu, L. Van Lich, and T. Q. Bui, "Functionally graded curved Timoshenko microbeams: A numerical study using IGA and modified couple stress theory," *Compos. Struct.*, vol. 254, p. 112841, Dec. 2020, doi: 10.1016/j.compstruct.2020.112841.

[41] A. Mouffoki, E. A. Adda Bedia, M. S. A. Houari, A. Tounsi, and S. R. Mahmoud, "Vibration analysis of nonlocal advanced nanobeams in hygro-thermal environment using a new two-unknown trigonometric shear deformation beam theory," *Smart Struct. Syst.*, vol. 20, no. 3, pp. 369–383, Sep. 2017, doi: 10.12989/sss.2017.20.3.369.

[42] Q. Li, D. Wu, W. Gao, F. Tin-Loi, Z. Liu, and J. Cheng, "Static bending and free vibration of organic solar cell resting on Winkler-Pasternak elastic foundation through the modified strain gradient theory," *Eur. J. Mech. A/Solids*, vol. 78, p. 103852, Nov. 2019, doi: 10.1016/j.euromechsol.2019.103852.

[43] M. Mosayyebi, F. Ashenai Ghasemi, and M. Aghaee, "Modified couple stress theory for wave propagation in viscoelastic sandwich microplates with FG-GPLRC core and piezoelectric face sheets as sensor and actuator," *Waves in Random and Complex Media*, 2022, doi: 10.1080/17455030.2022.2106387.

[44] S. Natarajan, M. Haboussi, and G. Manickam, "Application of higher-order structural theory to bending and free vibration analysis of sandwich plates with CNT reinforced composite facesheets," *Compos. Struct.*, vol. 113, no. 1, pp. 197–207, Jul. 2014, doi: 10.1016/j.compstruct.2014.03.007.

[45] W. Gao, Z. Qin, and F. Chu, "Wave propagation in functionally graded porous plates reinforced with graphene platelets," *Aerosp. Sci. Technol.*, vol. 102, p. 105860, Jul. 2020, doi: 10.1016/j.ast.2020.105860.

[46] M. Arefi, E. Mohammad-Rezaei Bidgoli, and T. Rabczuk, "Thermo-mechanical buckling behavior of FG GNP reinforced micro plate based on MSGT," *Thin-Walled Struct.*, vol. 142, pp. 444–459, Sep. 2019, doi: 10.1016/j.tws.2019.04.054.

[47] T. H. L. Bekkaye *et al.*, "Porosity-dependent mechanical behaviors of FG plate using refined trigonometric shear

deformation theory," *Comput. Concr.*, vol. 26, no. 5, pp. 439–450, Nov. 2020, doi: 10.12989/cac.2020.26.5.439.

[48] I. M. Mudhaffar, A. Chikh, A. Tounsi, M. A. Al-Osta, M. M. Al-Zahrani, and S. U. Al-Dulaijan, "Impact of viscoelastic foundation on bending behavior of FG plate subjected to hygro-thermo-mechanical loads ," *Struct. Eng. Mech.*, vol. 86, no. 2, p. 167, Apr. 2023, doi: 10.12989/SEM.2023.86.2.167.

[49] F. M. V. Ebrahimi, "Vibration analysis of magneto-flexo-electrically actuated porous rotary nanobeams considering thermal effects via nonlocal strain gradient elasticity theory," *Adv. nano Res.*, vol. 7, no. 4, pp. 223–231, 2019, doi: 10.12989/anr.2019.7.4.223.

[50] M. Mekerbi, S. Benyoucef, A. Mahmoudi, A. Tounsi, A. A. Bousahla, and S. R. Mahmoud, "Thermodynamic behavior of functionally graded sandwich plates resting on different elastic foundation and with various boundary conditions," *J. Sandw. Struct. Mater.*, p. 109963621985128, May 2019, doi: 10.1177/1099636219851281.

[51] S. J. Lee and J. N. Reddy, "Vibration suppression of laminated shell structures investigated using higher order shear deformation theory," *Smart Mater. Struct.*, vol. 13, no. 5, pp. 1176–1194, 2004, doi: 10.1088/0964-1726/13/5/022.

[52] T. Q. Bui *et al.*, "On the high temperature mechanical behaviors analysis of heated functionally graded plates using FEM and a new third-order shear deformation plate theory," *Compos. Part B Eng.*, vol. 92, pp. 218–241, May 2016, doi: 10.1016/j.compositesb.2016.02.048